Solar Energy Materials & Solar Cells 117 (2013) 564–568

Contents lists available at ScienceDirect

Solar Energy Materials & Solar Cells

journal homepage: www.elsevier.com/locate/solmat

Electrodeposited NiO anode interlayers: Enhancement of the charge carrier selectivity in organic solar cells

Teresa Ripolles-Sanchis [a], Antonio Guerrero [a], Eneko Azaceta [b], Ramon Tena-Zaera [b,*], Germà Garcia-Belmonte [a,**]

[a] Photovoltaic and Optoelectronic Devices Group, Departament de Física, Universitat Jaume I, ES-12071 Castelló, Spain
[b] Energy Division, IK4-CIDETEC, ES-20009 San Sebastian, Spain

ARTICLE INFO

Article history:
Received 24 May 2013
Received in revised form
11 July 2013
Accepted 12 July 2013

Keywords:
Organic photovoltaics
Nickel oxide
Hole transport layer
Charge carrier selectivity

ABSTRACT

Nickel oxide (NiO) thin films prepared by cathodic electrodeposition exhibit superior electrical performace than PEDOT:PSS when used as anode interlayers of bulk-heterojunction solar cells. Devices incorporating 30 nm-thick NiO films firstly annealed at 320 °C in air and posteriorly treated with UV-O_3 reach power conversion efficiencies comparable to that obtained for PEDOT:PSS-based cells. NiO interlayers enhance contact selectivity by simulataneously increasing shunt resistance (lower leakage current related to electron-blocking ability), and reducing hole-extraction resistance. Carrier selectivity is quantified from the resistance components associated with the impedance response of the anode contacts. The versatile electrodeposition technique of NiO interlayers permits avoiding PEDOT:PSS use as it presents disadvantages related to its acid character and hygroscopic nature.

1. Introduction

The increasing demand for renewable energy resources leads researchers to study different routes in solar energy production. Nowadays, organic bulk heterojunction (BHJ) solar cells are deeply investigated due to their potential to reduce fabrication costs. This is so because mechanical flexibility, light weight and manufacturing using solution-based processing as spray coating or inkjet printing, which are appealing for roll-to-roll production, make the technology highly attractive [1,2]. Up to now the maximum power conversion efficiency (PCE) is on the order of ~10% [3–7]. BHJ cells typically integrate blends formed by a donor polymer, such as poly (3-hexylthiophene) (P3HT) and an acceptor fullerene, such as [6,6]-phenyl-C61-butyric acid methyl ester ($PC_{60}BM$). Efficient electrodes comprise a transparent conducting oxide (TCO) anode, such as indium tin oxide (ITO), and a low work function metal cathode. A hole transport layer (HTL) is deposited between the TCO anode and bulk heterojunction layer to enhance hole extraction by reducing contact resistance, acting simultaneously as an electron-blocking layer. The most commonly employed HTL material in polymer solar cell is the copolymer poly(3,4-ethylenedioxythiophene):poly(styrenesulfonate) (PEDOT:PSS) [8], because it is insoluble in organic solvents, conductive, and highly transparent to visible light. However, PEDOT:PSS presents some disadvantages as its acid character (pH = 1.2) and hygroscopic nature cause corrosion of the ITO anode subsequently allowing indium diffusion throughout the device [9]. Other alternatives for an efficient anode interlayer material use wide band gap ($E_g \geq 3$ eV) *p*-doped materials such as several transition metal oxides (V_2O_5, MoO_3, and WO_3) [10–13] which are usually incorporated using less convenient vacuum deposition techniques. Therefore it would be necessary to investigate on HTL materials processed from solution routes. An ideal candidate can be nickel oxide (NiO). However it is known that NiO contact properties are highly sensitive to the surface chemistry, crystal orientation and thin film processing [7,14,15].

In this work, an efficient anode NiO interlayer is prepared on top of the ITO by a versatile cathodic electrochemical deposition method [16]. Surface treatments such as UV–ozone (UVO) and annealing treatment (AT) in air allows reducing contact resistance and simultaneously increasing shunt resistance, enhancing as a consequence photovoltaic parameters. In particular carrier selectivity of the anodes is quantified from the resistance components associated with the impedance response of the contacts. Compared to the PEDOT:PSS HTL, solar cells including NiO exhibit superior electrical characteristics (carrier selectivity $s > 99\%$).

2. Results and discussion

Two different HTLs were tested: namely PEDOT:PSS layers, and NiO films. PEDOT:PSS was spin coast onto ITO-coated glass substrate (10 Ω/sq) at 5500 rpm for 30 s, then 3000 rpm for 30 s in air.

* Corresponding author. Tel.:+ 34 943 309022.
** Corresponding author. Tel.:+ 34 964 387538.
E-mail addresses: rtena@cidetec.es (R. Tena-Zaera), garciag@uji.es (G. Garcia-Belmonte).

0927-0248/$ - see front matter © 2013 Elsevier B.V. All rights reserved.
http://dx.doi.org/10.1016/j.solmat.2013.07.020

The thickness of the PEDOT:PSS layer was about 30 nm, as determined by a VEECO DEKTACK 6M Stylus Profiler. To remove the traces of water, the substrates were heated at 130 °C for 10 min. NiO deposition on the ITO was performed from the electrochemical reduction of O_2 in an aprotic ionic liquid (i.e. 1-butyl-1-methylpyrrolidinium bis(trifluoromethanesulfonyl)imide, $PYR_{14}TFSI$)-based electrolyte containing nickel bis(trifluoromethanesulfonyl)imide (5×10^{-2} M). Further experimental details can be found elsewhere [16]. Charge densities of 13 and 25 mC/cm^2 were passed during the electrodeposition in order to obtain NiO films with thickness of 30 and 50 nm, respectively. Some of the obtained NiO samples were heated at 320 °C for 20 min (annealing treatment AT), and then UVO treatment were carried on for 10 min. Other 30 nm-thick NiO films were analyzed reversing the processing: firstly UVO treatment was performed and then submitted to AT with the same conditions as in the previous devices. Also 30 nm-thick NiO films were studied as-deposited without any post-treatments. The active layer consisting of P3HT and $PC_{60}BM$ blend was spin-cast in a glove box from orthodichlorobenzene (ODCB) solution on top of the HTL layer. The active layer was deposited at 1200 rpm for 10 s (100 nm-thick). The films were then annealed on a hot plate in the glove box at 130 °C for 10 min. Ca/Ag (5 nm/100 nm) cathodes were used as top electrodes by thermal evaporation. Devices of structure glass/ITO/HTL/P3HT:$PC_{60}BM$/Ca/Ag are analyzed by impedance spectroscopy (IS) technique under 1 sun illumination.

The morphology of NiO layers is analyzed by scanning electron microscopy. Although conformal-like ~30 nm thick coating of the ITO substrate is observed after electrodeposition experiments passing a charge density of 13 mC/cm^2 (Fig. 1b and d), a decrease of roughness – versus to the naked substrates (Fig. 1a) – can be inferred in samples obtained after applying 25 C/cm^2 (Fig. 1c). The decrease of the roughness for thicker layers was confirmed by atomic force microscopy [16]. The substrates coated with the different HTLs are characterized UV–vis spectra (Fig. 2), detecting significant changes in the transmittance of the NiO films as-deposited and after each treatment. The differences suggest changes in the NiO stoichiometry. A similar high transmittance is observed for the as-deposited and after UVO/AT treatments of 30 nm-thick NiO films and PEDOT:PSS film. Transmittance lowers when AT/UVO is performed on NiO films with different thicknesses 30 and 50 nm. This transmittance reduction is reflected in the photovoltaic characteristics as discussed later. Previous research informs that the work function of NiO is strongly dependent on the thickness, O_2-plasma, and annealing treatments [17]. For example, a O_2-plasma treatment increases the work function of NiO, by forming NiO_x layers with their electronic properties dictated by the formation of metal cation vacancies, and regions in the oxide lattice which are rich in oxygen [17]. Also deposition methods such as pulsed laser deposition, sol–gel route, or sputtering play a determining role [9,18]. We consider here that UVO treatment followed in our experiments produces similar effects as those occurring after O_2-plasma treatment [18]. Furthermore, recent research reveals that ozone exposure increased the Ni oxidation state by introducing hole states, giving rise to higher-performance aluminum-coated NiO films [19].

The electrical properties of the glass/ITO/HTL/P3HT:$PC_{60}BM$/Ca/Ag solar cells are shown as current density–voltage $j-V$ characteristics under simulated AM1.5G illumination (1000 W m^{-2}) (Fig. 3a). The photovoltaic parameters for PEDOT:PSS and all NiO interlayer-based devices are summarized in Table 1. It is clearly observed that the NiO as-deposited device has the lowest photovoltaic parameters (see Table 1) indicating that surface treatments are necessary to improve contact conditions. When NiO films are annealed before UVO treatment, the open-circuit voltage yields ~620 mV (see Table 1), a value similar to that achieved with PEDOT:PSS. However 30 nm-thick NiO-based device with firstly UVO treatment (UVO/AT) only yields 260 mV (see Table 1). Reduction in open-circuit voltage suggests that the NiO film with the

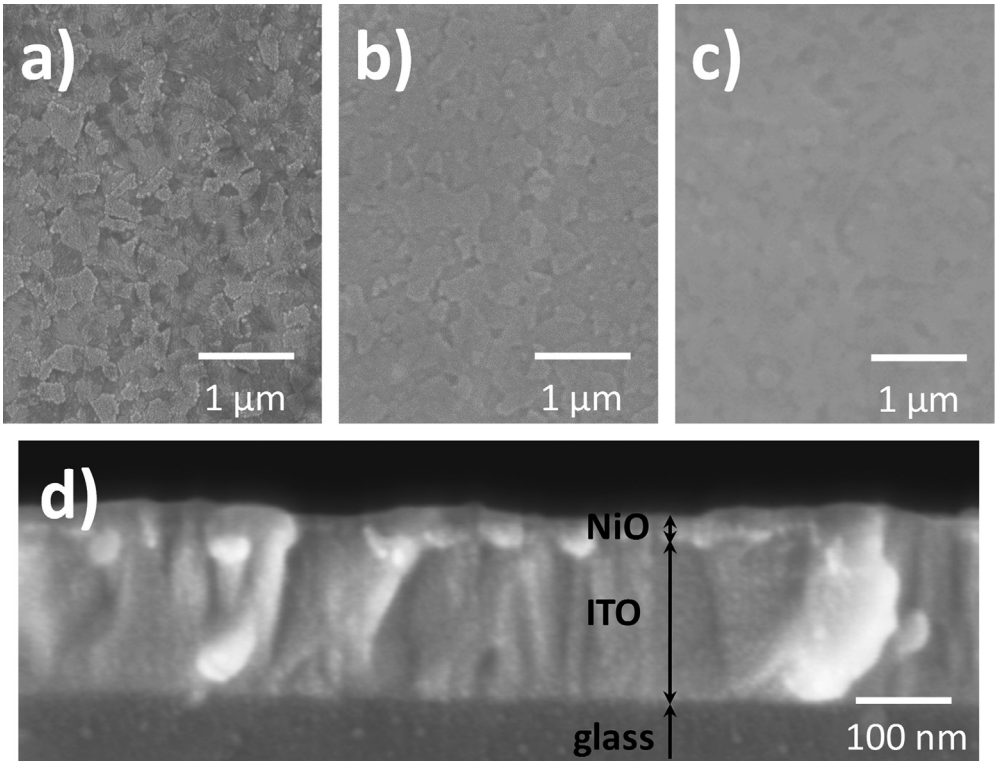

Fig. 1. Top view SEM micrographs of a naked ITO substrate (a) and NiO layers electrodeposited by passing a charge density of 13 (b) and 25 mC/cm^2 (c). The figure (d) shows a cross section SEM micrograph of the sample showed in figure (b).

previous UVO treatment exhibits blocking characteristics as next explained in describing impedance spectroscopy results. The optimum observed photovoltaic result corresponds to the 30 nm-thick NiO treated with UVO after annealing the interlayer.. This results in an power conversion efficiency of 3.44%, comparable to a common device with PEDOT:PSS. The main difference between these two cells is the short-circuit current j_{sc} and EQE response (Fig. 3b). The lower j_{sc} for the 30 nm-thick NiO (AT/UVO) solar cell is attributed to the lower transmittance spectra as observed in Fig. 1. However NiO-based cell exhibits an improved fill factor (FF) in comparison to PEDOT:PSS-based cell (see Table 1). FF is known to be connected to resistive effects, either in series or in parallel, which limits the electrical power delivered by a solar cell. Improvement in contact resistive effects derives from the capacity of the outer anode interface for simultaneous (*i*) hole extraction and (*ii*) electron blocking, a feature that states the contact selectivity [20]. We next use impedance spectroscopy to discern out the origin of such FF increment.

Impedance spectroscopy (IS) is an experimental technique able to separate different resistive and capacitance contributions to the overall solar cell electrical response [21]. NiO-based devices and a standard device with PEDOT:PSS as HTL are studied by IS under 1 sun irradiation intensity by varying bias voltage. $Z'-Z''$ plots exhibit a typical impedance response of organic solar cells displaying two arcs (see Fig. 3) [22,23]. The equivalent circuit model shown in Fig. 4 provides a high quality fit of the data for all devices. At lower frequencies, a large arc dominates in the $Z'-Z''$ plot which is represented by a *RC* subcircuit. This part is related to the recombination resistance R_{rec}, derivative of the carrier recombination flux; and the chemical capacitance C_μ related to carrier

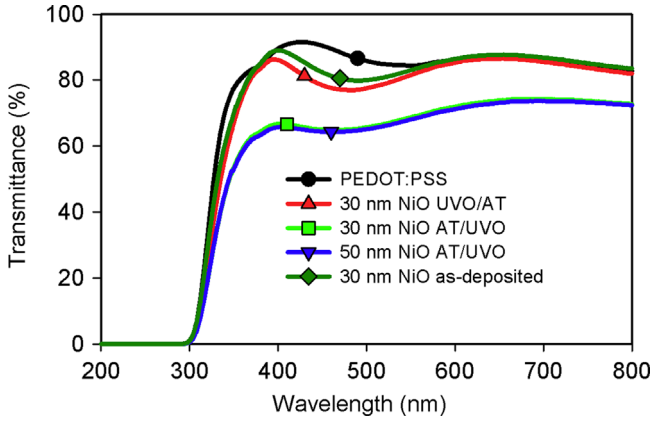

Fig. 2. Transmission spectra of HTL films on top of ITO substrates. The HTL analyzed were PEDOT:PSS film and NiO films treated by the following ways: as-deposited (30 nm), AT/UVO (30 and 50 nm) and UVO/AT (30 nm).

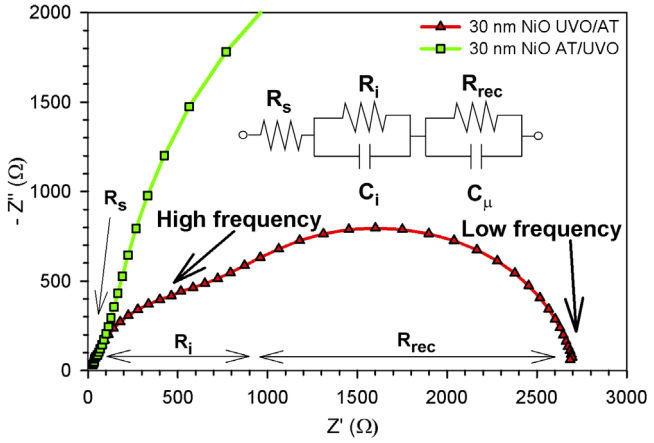

Fig. 4. $Z'-Z''$ plot of 30 nm-thick NiO UVO/AT and AT/UVO-based solar cell at 300 mV-bias voltage under 1 sun illumination. The equivalent circuit model is also indicated, which comprises a series resistance R_s, interlayer resistance R_i, interlayer capacitance C_i, recombination resistance R_{rec}, and chemical capacitance C_μ.

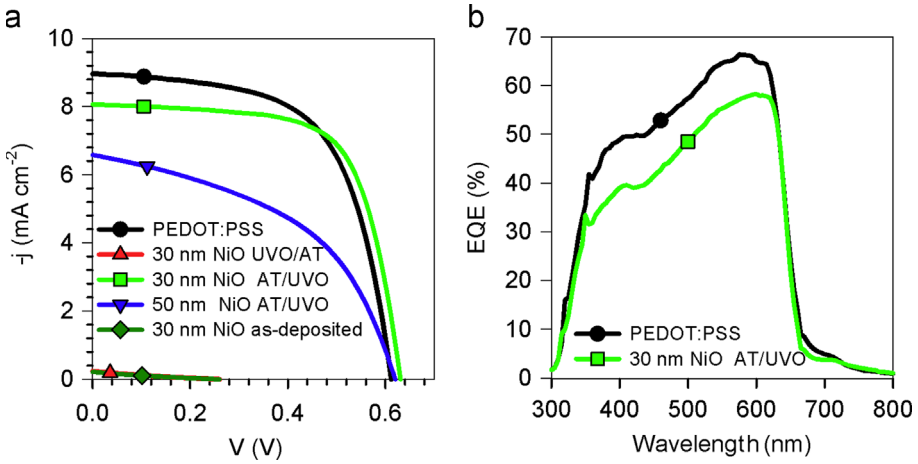

Fig. 3. (a) Current density–voltage plots under 1 sun illumination for glass/ITO/HTL/P3HT:PC_{60}BM/Ca/Ag BHJ solar cells fabricated with PEDOT:PSS (standard device) and NiO films (as-deposited, AT/UVO and UVO/AT for 30 nm thick and 50 nm thick for AT/UVO). (b) EQE spectra of glass/ITO/PEDOT:PSS or 30 nm NiO (AT/UVO)/P3HT:PC_{60}BM/Ca/Ag devices.

Table 1
Photovoltaic characteristics for P3HT:PC_{60}BM solar cells with PEDOT:PSS and NiO interlayers. AT=annealing treatment.

HTL	HTL thickness, nm	Process	j_{sc}, mA cm^{-2}	V_{oc}, mV	FF, %	PCE, %	Selectivity, %
PEDOT:PSS	30	standard	8.97	611	62	3.39	95.0
NiO	30	UVO/AT	0.42	260	19	0.02	–
NiO	30	AT/UVO	8.06	630	67	3.44	99.6
NiO	50	AT/UVO	6.58	620	47	1.92	85.0
NiO	30	as-deposited	0.20	258	23	0.01	–

storage [21]. At higher frequencies, an additional arc is clearly observed in the Z′–Z″ plot for the 30 nm-thick NiO (UVO/AT)-based solar cell (Fig. 4). This high-frequency arc is also visible, although to a minor extent, with the other devices (shown in Fig. 4 for 30 nm-thick NiO (AT/UVO)-based device). This extra arc at high frequencies is represented by a parallel *RC* which is directly dependent on the HTL/active layer interface. It is interpreted in terms of an interlayer resistance R_i, and capacitance C_i. The equivalent circuit model also has a series resistance R_s resulting from the electrode contacts.

IS parameters extracted from fitting of the Nyquist plots using the equivalent circuit model showed in Fig. 4 are shown in Fig. 5. NiO (UVO/AT)-based device show a voltage-independent, high R_i~70 Ω cm^2 (Fig. 5a). This is a considerable resistance that contributes to hinder hole extraction at the anode contact. We had studied a similar blocking-like behavior with a CaO layer at the cathode [23]. Performing annealing treatment before UVO seems necessary to reduce the contact resistance. This is likely due to a better matching in the energy levels at the interface. Thicker NiO interlayers (50 nm AT/UVO) exhibit intermediate R_i values (~30 Ω cm^2) in comparison to those obtained with thinner NiO (30 nm AT/UVO) and PEDOT:PSS (< 10 Ω cm^2). It is interesting to note that R_i for these last cells contributes similarly to the overall series resistance. However the thinner NiO-layer cell presents lower R_i values around the maximum power point. This explains in part the increment in FF exhibited by the NiO-based cell (see Table 1). Other possible factors influencing FF are originated by recombination currents (represented by R_{rec}), and leakage current (modeled by the shunt resistance R_{sh}) determining the slope of the j–V curves near short circuit.

The recombination resistance R_{rec} (Fig. 5b) follows the expected decreasing behavior at forward voltage due to the enhancement of the recombination current [21]. At low voltages R_{rec} tends to saturate because the differential resistance measured is not determined by the recombination flux but by a shunt resistance R_{sh} caused by additional leakage currents flowing in parallel [22]. In that region, R_{sh} corresponding to the 30 nm NiO (AT/UVO) solar cell is higher than that exhibited by other devices. This effect is reflected in the j–V curve which has a nearly flat response at low voltages. At higher voltages, R_{rec} shows similar decreasing behavior for the working devices (PEDOT:PSS and 30 nm-thick NiO AT/UVO). This fact precludes connecting the differences in FF to recombination currents occurring within the active layer bulk. On the contrary large R_{sh} variations (from ~200 Ω cm^2 with PEDOT:PSS to ~3 kΩ cm^2 with thin NiO AT/UVO) are directly linked with the increment in FF, which finally improves performance. The interplay between hole extraction (low R_i values) and leakage current blocking (high R_{sh}) is used to define the carrier selectivity degree exhibited by the anode contact. We propose that the contact selectivity can simply be expressed as

$$s = 1 - \frac{R_i}{R_{sh}} \quad (1)$$

which results in $s = 1$ for a fully selective contact. Selectivity values are summarized in Table 1. It is noted that s correlates with FF as expected. The definition of contact selectivity in Eq. (1) tries to capture the balance between the charge (hole) extraction ability of the anode and the detrimental leakage current flowing in parallel to the photocurrent. The ratio between R_i and R_{sh} compares the anode opposition to the hole extraction in the energy-generating quadrant of the j–V curve and the resistance caused by the leakage current.

The capacitance plot C_μ (Fig. 5d) of the 30 nm-thick NiO (AT/UVO) and PEDOT:PSS-based devices exhibits at higher voltages the expected increase as fullerene states are occupied toward forward bias [21]. The 30 nm-thick NiO (UVO/AT) cell shows a voltage-independent C_μ under illumination related to the blocking behavior which approximately corresponds to the chemical capacitance found for working cells at V_{app}≈400 mV. A similar behavior was found when insulating layer were intentionally deposited at the cathode contact [23]. At lower voltages all devices exhibit the expected capacitive response originated by the modulation of the depletion zone built up at the cathode contact, which collapses to the geometrical capacitance near zero voltage [24]. Finally Fig. 5c represents C_i versus applied voltage. The 30 nm-thick NiO (AT/UVO) and PEDOT:PSS HTL-based OPV devices have the same behavior which increases toward forward bias. On the contrary the other devices exhibit almost constant, lower C_i values. The transition between low to high C_i appears to be connected to the change between dielectric to charge accumulation mechanisms at the interlayer.

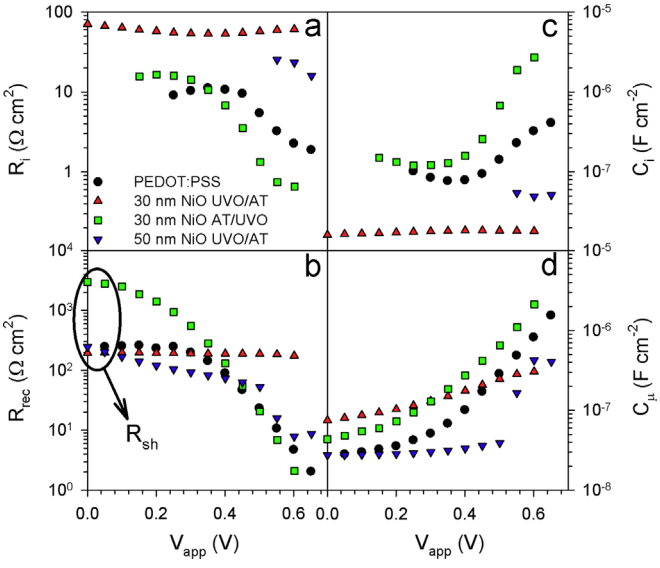

Fig. 5. (a) Interlayer resistance R_i, (b) recombination resistance R_{rec}, (c) interlayer capacitance C_i, and (d) chemical capacitance C_μ as a function of the applied voltage extracted from the fitting of the equivalent circuit model shown in Fig. 3.

3. Conclusions

We finally remark that NiO electrodeposition from aprotic ionic liquids appears to be a viable vacuum-free approach to integrate HTL in BHJ solar cells in a single-step process i.e. avoiding the post-deposition thermal treatments needed in the aqueous-based electrodeposition [15], and the consequent traces of nickel hydroxide-related phases present even after annealing treatments [25]. Surface treatments such as UVO and annealing treatment have an important effect on the electrical behavior of the NiO as anode interlayer. Different thicknesses (30 and 50 nm) and treatment order (AT/UVO or UVO/AT) have been studied in the conventional device architecture of organic solar cells. The efficiency values of the device prepared with 30 nm-thick NiO film (AT/UVO) HTL is comparable with a standard PEDOT:PSS. NiO interlayers present a superior electrical response as evidenced by the reduction in the overall series resistance, and larger shunt resistance. These two parameters allow explaining the higher FF observed for 30 nm-thick NiO AT/UVO films. The proposed analytical technique based on IS can be further used when different contact structures are compared, allowing for a quantification of the carrier selectivity.

Acknowledgments

We thank financial support from Generalitat Valenciana (Prometeo/2009/058, and ISIC/2012/008 Institute of Nanotechnologies for Clean Energies), and FP7 European Project ORION (Large CP-

IP229036-2). R.T.-Z. acknowledges the support of the Program "Ramón y Cajal" of the MICINN.

References

[1] F.C. Krebs, S.A. Gevorgyan, B. Gholamkhass, S. Holdcroft, C. Schlenker, M.E. Thompson, B.C. Thompson, D. Olson, D.S. Ginley, S.E. Shaheen, H.N. Alshareef, J.W. Murphy, W.J. Youngblood, N.C. Heston, J.R. Reynolds, S.J. Jia, D. Laird, S.M. Tuladhar, J.G.A. Dane, P. Atienzar, J. Nelson, J.M. Kroon, M.M. Wienk, R.A.J. Janssen, K. Tvingstedt, F.L. Zhang, M. Andersson, O. Inganas, M. Lira-Cantu, R. de Bettignies, S. Guillerez, T. Aernouts, D. Cheyns, L. Lutsen, B. Zimmermann, U. Wurfel, M. Niggemann, H.F. Schleiermacher, P. Liska, M. Gratzel, P. Lianos, E.A. Katz, W. Lohwasser, B. Jannon, A round robin study of flexible large-area roll-to-roll processed polymer solar cell modules, Solar Energy Materials and Solar Cells 93 (2009) 1968–1977.

[2] F.C. Krebs, Fabrication and processing of polymer solar cells: a review of printing and coating techniques, Solar Energy Materials and Solar Cells 93 (2009) 394–412.

[3] M.C. Scharber, D. Mühlbacher, M. Koppe, P. Denk, C. Waldauf, A.J. Heeger, C.J. Brabec, Design rules for donors in bulk-heterojunction solar cells—towards 10% energy-conversion efficiency, Advanced Materials 18 (2006) 789–794.

[4] Y. Sun, C.J. Takacs, S.R. Cowan, J.H. Seo, X. Gong, A. Roy, A.J. Heeger, Efficient, air-stable bulk heterojunction polymer solar cells using MoOx as the anode interfacial layer, Advanced Materials (Weinheim, Germany) 23 (2011) 2226–2230.

[5] S. Chen, C.E. Small, C.M. Amb, J. Subbiah, T.H. Lai, S.W. Tsang, J.R. Manders, J.R. Reynolds, F. So, Inverted polymer solar cells with reduced interface recombination, Advanced Energy Materials 2 (2012) 1333–1337.

[6] W. Chen, M.P. Nikiforov, S.B. Darling, Morphology characterization in organic and hybrid solar cells, Energy and Environmental Science 5 (2012) 8045–8074.

[7] L. Dou, J. You, J. Yang, C.-C. Chen, Y. He, S. Murase, T. Moriarty, K. Emery, G. Li, Y. Yang, Tandem polymer solar cells featuring a spectrally matched low-bandgap polymer, Nature Photonics 6 (2012) 180–185.

[8] G. Greczynski, T. Kugler, M. Keil, W. Osikowicz, M. Fahlman, W.R. Salaneck, Photoelectron spectroscopy of thin films of PEDOT-PSS conjugated polymer blend: a mini-review and some new results, Journal of Electron Spectroscopy and Related Phenomena 121 (2001) 1–17.

[9] K.X. Steirer, J.P. Chesin, N.E. Widjonarko, J.J. Berry, A. Miedaner, D.S. Ginley, D.C. Olson, Solution deposited NiO thin-films as hole transport layers in organic photovoltaics, Organic Electronics 11 (2010) 1414–1418.

[10] S. Schubert, M. Hermenau, J. Meiss, L. Müller-Meskamp, K. Leo, Oxide sandwiched metal thin-film electrodes for long-term stable organic solar cells, Advanced Functional Materials 22 (2012) 4993–4999.

[11] J. Meyer, S. Hamwi, M. Kroger, W. Kowalsky, T. Riedl, A. Kahn, Transition metal oxides for organic electronics: energetics, device physics and applications, Advanced Materials 24 (2012) 5408–5427.

[12] H.-Q. Wang, N. Li, N.S. Guldal, C.J. Brabec, Nanocrystal V_2O_5 thin film as hole-extraction layer in normal architecture organic solar cells, Organic Electronics 13 (2012) 3014–3021.

[13] E.L. Ratcliff, B. Zacher, N.R. Armstrong, Selective inter layers and contacts in organic photovoltaic cells, Journal of Physical Chemistry Letters 2 (2011) 1337–1350.

[14] M.D. Irwin, J.D. Servaites, D.B. Buchholz, B.J. Leever, J. Liu, J.D. Emery, M. Zhang, J.H. Song, M.F. Durstock, A.J. Freeman, M.J. Bedzyk, M.C. Hersam, R.P.H. Chang, M.A. Ratner, T.J. Marks, Structural and electrical functionality of NiO interfacial films in bulk heterojunction organic solar cells, Chemistry of Materials 23 (2011) 2218–2226.

[15] H. Yang, C. Gong, G.H. Guai, C.M. Li, Organic solar cells employing electro-deposited nickel oxide nanostructures as the anode buffer layer, Solar Energy Materials and Solar Cells 101 (2012) 256–261.

[16] E. Azaceta, S. Chavhan, P. Rossi, M. Paderi, S. Fantini, M. Ungureanu, O. Miguel, H.-J. Grande, R. Tena-Zaera, NiO cathodic electrochemical deposition from an aprotic ionic liquid: building metal oxide n–p heterojunctions, Electrochimica Acta 71 (2012) 39–43.

[17] K.X. Steirer, P.F. Ndione, N.E. Widjonarko, M.T. Lloyd, J. Meyer, E.L. Ratcliff, A. Kahn, N.R. Armstrong, C.J. Curtis, D.S. Ginley, J.J. Berry, D.C. Olson, Enhanced efficiency in plastic solar cells via energy matched solution processed NiOx interlayers, Advanced Energy Materials 1 (2011) 813–820.

[18] E.L. Ratcliff, J. Meyer, K.X. Steirer, A. Garcia, J.J. Berry, D.S. Ginley, D.C. Olson, A. Kahn, N.R. Armstrong, Evidence for near-surface NiOOH species in solution-processed NiOx selective interlayer materials: impact on energetics and the performance of polymer bulk heterojunction photovoltaics, Chemistry of Materials 23 (2011) 4988–5000.

[19] F. Lin, D. Nordlund, T.-C. Weng, R.G. Moore, D.T. Gillaspie, A.C. Dillon, R.M. Richards, C. Engtrakul, Hole doping in Al-containing nickel oxide materials to improve electrochromic performance, ACS Materials & Interfaces 5 (2013) 301–309.

[20] A. Guerrero, B. Dörling, T. Ripolles-Sanchis, M. Aghamohammadi, E. Barrena, M. Campoy-Quiles, G. Garcia-Belmonte, Interplay between fullerene surface coverage and contact selectivity of cathode interfaces in organic solar cells, ACS Nano 7 (2013) 4637–4646.

[21] G. Garcia-Belmonte, A. Guerrero, J. Bisquert, Elucidating operating modes of bulk-heterojunction solar cells from impedance spectroscopy analysis, Journal of Physical Chemistry Letters 4 (2013) 877–886.

[22] A. Guerrero, L.F. Marchesi, P.P. Boix, J. Bisquert, G. Garcia-Belmonte, Recombination in organic bulk heterojunction solar cells: small dependence of interfacial charge transfer kinetics on fullerene affinity, Journal of Physical Chemistry Letters 3 (2012) 1386–1392.

[23] T. Ripolles-Sanchis, A. Guerrero, J. Bisquert, G. Garcia-Belmonte, Diffusion–recombination determines collected current and voltage in polymer:fullerene solar cells, Journal of Physical Chemistry C 116 (2012) 16925–16933.

[24] A. Guerrero, L.F. Marchesi, P.P. Boix, S. Ruiz-Raga, T. Ripolles-Sanchis, G. Garcia-Belmonte, J. Bisquert, How the charge–neutrality level of interface states controls energy level alignment in cathode contacts of organic bulk-heterojunction solar cells, ACS Nano 6 (2012) 3453–3460.

[25] E. Azaceta, N.T. Tuyena, D.F. Pickup, C. Rogero, E. Ortega, O. Miguel, H.-J. Grande, R. Tena-Zaera, One-step wet chemical deposition of NiO from the electrochemical reduction of nitrates in ionic liquid based electrolytes, Electrochimica Acta 96 (2013) 261–267.